JPET Fast Forward. Published on September 9, 2019 as DOI: 10.1124/jpet.119.261347
This article has not been copyedited and formatted. The final version may differ from this version.

JPET # 261347

Direct measurement of kinetic parameters of ABCG2-dependent transport of natural flavonoids using a fluorogenic substrate

Michal Rozanski, Maciej Studzian, Lukasz Pulaski

Laboratory of Transcriptional Regulation, Institute of Medical Biology, Polish Academy of Sciences, Lodowa 106, 93-232 Lodz, Poland (MR, LP)

Department of Molecular Biophysics, Faculty of Biology and Environmental Protection, University of Lodz, 12/16 Banacha St., 90-237 Lodz, Poland (MS, LP)

Department of Molecular Biology of Cancer, Medical University of Lodz, Lodz, Poland (MR)

JPET # 261347

Running title: Direct measurement of ABCG2-dependent flavonoid transport

Address correspondence to: Lukasz Pulaski, Institute of Medical Biology PAS, Lodowa 106, 93-232 Lodz, Poland, lpulaski@uni.lodz.pl

Number of text pages: 29

Number of tables: 2

Number of figures: 5

Number of references: 49

Number of words in the Abstract: 228

Number of words in the Introduction: 626

Number of words in the Discussion: 2029

Non-standard Abbreviations:

ABC - ATP binding cassette; APB - 2-aminoethyl diphenylborinate ; BSA - Bovine serum albumin; DMEM - Dulbecco's Modified Eagle Medium; HBSS - Hanks's Balanced Salt Solution; LB - Lysis Buffer; LC-MS - Liquid chromatography–mass spectrometry; PBS - Phosphate buffered saline;

Recommended section assignment:

Metabolism, Transport, and Pharmacogenomics

Abstract

Flavonoids are an important part of the human diet as plant-derived polyphenols and the mechanisms governing their pharmacokinetics are important both due to their own nutriceutical activity and due to the potential for food-drug interactions. A central determinant of absorption and distribution of flavonoids in the human body is the ABC transporter ABCG2, expressed in gut epithelium and in other barrier tissues. While flavonoids were previously identified as substrates and/or inhibitors of this protein, precise enzyme kinetic calculations of affinity and activity parameters are rare due to the lack of suitable experimental models. We present a novel method which allows the direct measurement of kinetic constants for ABCG2-mediated cellular efflux of natural flavonoids thanks to the application of fluorogenic 2-aminoethyl diphenylborinate (APB) which reacts with intracellular flavonoids forming a fluorescent, non-membrane-permeable conjugate, thus making it possible to measure the intracellular substrate concentration throughout the experiment. Our studies were performed in MDCKII-derived cell lines expressing human ABCG2 and involve substrate efflux from whole, unmodified cells, precluding the need for plasma membrane vesicle preparation. We present methods for calculation of enzyme kinetic constants by measuring substrate concentration at efflux-influx equilibrium or during efflux from pre-loaded cells – we obtained Km values of 137 μM for quercetin, 36 μM for kaempferol and 348 μM for luteolin. Our method allows also direct verification of transport inhibition mechanism and potentially structure-activity relationship in substrates.

Significance Statement

The study presents the first direct calculation of kinetic constants for enzyme-mediated active transport of natural flavonoids in a whole-cell assay, using a fluorogenic compound to measure intracellular substrate concentrations at specific time points. It has implications for nutriceutical use of polyphenols, mechanisms of food-drug interactions and studies on absorption/distribution-determining membrane transporters, allowing a quantitative approach to pharmacokinetics of flavonoid transport across barrier tissues.

Introduction

Proteins of the ABC superfamily are membrane efflux transporters, actively pumping out xenobiotics outside of the cell (Ford and Beis, 2019). One among the best known ABC proteins is ABCG2, also known as Breast Cancer Resistance Protein (BCRP). ABCG2 is a so called half-transporter, which means that it is a homodimer of which each subunit (polypeptide chain) contains one nucleotide binding domain (ATP Binding Casette – ABC) and a hexahelical transmembrane domain. The spatial structure of human ABCG2 was resolved recently via cryo-electron microscopy (Taylor *et al.*, 2017). Physiologically, ABCG2 is expressed mainly in barrier tissues such as intestine (Sawangrat *et al.*, 2019), placenta (Mao, 2008; Szilagyi *et al.*, 2019) or blood-brain barrier (Iorio *et al.*, 2016) and significantly affects pharmacokinetics of many drugs (Shugarts and Benet, 2009; Robey *et al.*, 2011).

While precise biochemical knowledge about ABC transporters is extremely helpful in predicting their physiological relevance, e.g. for drug-drug interactions (International Transporter Consortium *et al.*, 2010), determining basic kinetic constants for active membrane transporters has always been a demanding task. Direct measurements of concentration of complex organic substrates (like anti-cancer drugs) are dependent on availability of radioactively labeled compounds or require sophisticated and artifact-prone methods like LC-MS (Xie *et al.*, 2015; Li *et al.*, 2017). Therefore, researchers often use model substrates, which can be detected more easily using fluorimetric, colorimetric or enzymatic assays. It is also common to measure the ATPase activity of the nucleotide binding domain instead of the transporter activity itself (Glavinas *et al.*, 2007).

When values of enzyme kinetic constants are required for ABC proteins, three approaches are predominant in the literature. The first one involves measuring equilibrium concentrations of a substrate on the apical and basolateral side of a cellular monolayer (Mukkavilli *et al.*, 2017). This assay depends on membrane domain-specific expression of the protein of interest in polarized cell lines. The second approach depends on the use of isolated membrane vesicles containing transporter molecules (Pedersen *et al.*, 2017). These methods often depend on heterologous overexpression of transporters, usually in insect cell lines. The third approach uses bioinformatic

modeling for prediction of kinetic parameters for a new substrate (Gantner *et al.*, 2017) or to build *in silico* transport models (Schutte *et al.*, 2006).

In this article we present the direct measurement of enzyme kinetic constants for ABCG2 with regard to flavonoids as natural substrates. They are ubiquitous polyphenolic plant secondary metabolites, abundant in diet and with many recognized bioactivities in the human body (Fraga *et al.*, 2019). Many of them are known or predicted to be substrates of the ABCG2 transporter (An *et al.*, 2011; Ge *et al.*, 2016; Iriti *et al.*, 2017; Sjöstedt *et al.*, 2017; Xiang *et al.*, 2018). Intestinal expression of ABCG2 defines it as one of crucial determinants of absorption and distribution of dietary compounds, and also as the primary location of food-drug and drug-drug pharmacokinetic interactions. While facilitated flavonoid transport has been described for some mammalian transporters from the SLC superfamily, such as glucose transporters (GLUT1, 2 and 4) or organic anion transporters (OAT1), only ABC transporters (ABCG2 and ABCB1) have been demonstrated to catalyze active flavonoid efflux (Passamonti *et al.*, 2009; Williamson *et al.*, 2018).

In this study, we apply the fluorogenic probe 2-aminoethyl diphenylborinate (APB, otherwise known as DPBA) in a dual role: to fix flavonoids inside the cells, preventing their further transport, and to measure their intracellular concentration directly by fluorimetry. The rationale of this method has been previously described by us (Sadowska-Bartosz *et al.*, 2016; Studzian and Pulaski, 2017), while here we modify and optimize it to allow the direct derivation of kinetic constants of transport. This method requires a stringently defined cellular model – in our case, a commercially available MDCKII-derived cell line pair which differs exclusively in the expression of human ABCG2.

Materials and methods

Cell culture

We used MDCKII-derived cell lines (Hera Biolabs, Lexington, KY, USA) which have a CRISPR/Cas9-mediated inactivation of canine *abcg2* and *abcb1* genes. The cell lines were: MDCKII-BP-null™ (control line, designated MDCK-WT) and hBCRP-MDCKII-BP-null™ (cell line stably transfected with the human *ABCG2* gene, designated MDCK-G2) [https://www.herabiolabs.com/mdck-bp-null-cells/]. Cell culture was performed in standard conditions (37°C, 5% CO_2). Cells were maintained in DMEM medium (Life Technologies) supplemented with Glutamax™ and 10% FBS (PAN - Biotech), without antibiotics.

Stock solutions, buffers

2-Aminoethyl diphenylborinate (APB) was purchased from Sigma, dissolved in DMSO to a concentration of 125 mg/ml and was stored at -20°C. Flavonoid stock solutions were prepared at concentration of 25 mM in DMSO and stored at -20°C. Working solutions were prepared in Dulbecco's Modified Eagle's Medium (DMEM, Life Technologies), in Hanks's Balanced Salt Solution (HBSS, Life Technologies) or in Phosphate Buffered Saline (PBS, Sigma-Aldrich). In some cases, bovine serum albumin (BSA, Sigma-Aldrich) or fatty acid-free BSA (FAF-BSA, Sigma-Aldrich) was included in solutions at a concentration of 2 mg/ml. Lysis buffer (LB) was prepared by dissolving APB from the stock solution to a final concentration of 250 µg/ml and Triton X-100 to a final concentration of 0.35%$_{v/v}$ in PBS.

Fluorescence measurement

24 h before the experiment, MDCKII cells were plated on a standard black 96-well plate at the density of 40000 cells per well. Flavonoids were dissolved from a stock solution to a desired concentration in HBSS/BSA. Cell culture medium was removed and cells were washed briefly with PBS at RT, then PBS was replaced with 100 µl of flavonoid solution. From this point on, the whole experiment was conducted in a thermostated glove chamber (Whitley H35 Hypoxystation, Don Whitley Scientific) with controlled atmosphere (37°C, 5% CO_2). Cells were incubated with

flavonoids for 40 min (until equilibrium was reached). For equilibrium concentration measurement, flavonoid solutions were replaced with 100 µl of PBS/APB. For kinetic (efflux) concentration measurement, flavonoid solutions were first replaced by 100 µl of DMEM/BSA and subsequently (after specific time periods) by same volume of PBS/APB. In both cases, cells were incubated with PBS/APB for 10 min and then washed once with PBS. PBS was carefully removed and cells were lysed with 100 µl of LB. After 5 min of incubation at RT, the plate was placed in EnVision 2103 multi-mode reader (PerkinElmer), shaken for 5 min and fluorescence intensity was measured at 550 nm emission and 485 nm excitation wavelengths. Independently, the fluorescence of a dilution series of flavonoids in LB was measured at the same conditions.

Protein assay

Bradford reagent was prepared by dissolving 50 mg of Coomassie Brilliant Blue G250 in 25 ml of methanol, then adding 50 ml of concentrated phosphoric (V) acid. Next, solution was diluted with milliQ water up to 500 ml and filtered. Bradford reagent was aliquoted into a clear 96-well plate (200 µl per well). Then 5 µl of a cellular lysate sample or 5 µl of lysis buffer (blank) were added to each well and thoroughly mixed. After 2 minutes of incubation at RT, the plate was placed in EnVision 2103 reader, shaken for a minute and absorbance was measured at 450 nm and 590 nm. Protein concentration in a sample is directly proportional to the ratio of 590 nm to 450 nm absorbance (Ernst and Zor, 2010).

Flavonoid concentration calculation

In order to calculate the intracellular flavonoid concentration, a measure of total cell volume in the well is necessary. We found that while volume of individual MDCKII cells can fluctuate depending on culture state and cell subline, the protein concentration in cell content is constant. Using the Bradford protein assay and optical microscope with Neubauer improved cell counting chamber we determined the ratio of cell volume to protein mass for both MDCKII sublines to be 14.5 µl/mg (data not shown). Thus, average intracellular concentration of flavonoids can be described with following equation:

$$C_{flavo.in\ cells} = \frac{C_{flavo.}}{C_{prot.} \cdot 14.5}\ [\mu M]$$

Where: $C_{flavo.}$ - flavonoid concentration in a well after lysis [μM], calculated from fluorescence values and the calibration curve; $C_{prot.}$ – protein concentration in a well after lysis [μg/ml]; 14.5 – cell volume to protein mass coefficient.

Measurement of passive transport constant

Passive transport of flavonoids through the plasma membrane can be described by first order kinetics. To measure the kinetic constant k, MDCK-WT cells were incubated to equilibrium with flavonoids and their intracellular (initial) concentration was measured. These cells contain no known active flavonoid transporters, since the expression of Abcg2 and Abcb1 has been genetically disrupted, and the known facilitated flavonoid transporters from the SLC superfamily that are expressed in these cells, such as Glut2 and Oat1, are expected to have a negligible contribution to passive flavonoid flux in view of the high unfacilitated (flip-flop) transport rate for the investigated flavonoids (aglycons, which are substantially less polar than flavonoid glycosides). Subsequently, a kinetic measurement was performed as described above by replacing the HBSS/BSA/flavonoid solution by DMEM/BSA and measuring intracellular concentration at specific time points. A first order substrate decay curve, described by the equation below, was fitted to experimental points using the least squares method.

$$C_{WT} = C_0 \cdot e^{-k \cdot t}$$

Where: C_{WT} – intracellular flavonoid concentration in MDCK-WT cells [μM]; C_0 - initial concentration [μM]; k – first order kinetic constant [1/s]; t- time [s]

Calculation of K_m and V_{max} for ABCG2 from equilibrium data

The availability of two cell lines which are identical in everything except ABCG2 expression makes it possible to derive the velocity of ABCG2-mediated flavonoid transport from intracellular concentration values at equilibrium. The derivation is based on the following premises:

1. Passive diffusion through membranes is a first-order process driven by the concentration of flavonoid on each side of the membrane.

JPET Fast Forward. Published on September 9, 2019 as DOI: 10.1124/jpet.119.261347
This article has not been copyedited and formatted. The final version may differ from this version.

2. At equilibrium, the net flavonoid flux through the membrane is equal to zero (influx and efflux velocities are equal). In MDCK-WT cells, that equilibrium can be described by the equation:

$$V_{WTpas.in} = V_{WTpas.eff}$$

Where: $V_{WTpas.in}$ – velocity of a passive influx; $V_{WTpas.out}$ – velocity of a passive efflux

In MDCK-G2 cells, where an active efflux component appears alongside passive efflux, this equation takes the form:

$$V_{G2pas.in} = V_{G2pas.eff} + V_{ABCG2}$$

Where: $V_{G2pas.in}$ – velocity of a passive influx; $V_{G2pas.out}$ – velocity of a passive efflux; V_{ABCG2} – velocity of a ABCG2 mediated, active transport.

3. The presence of active efflux shifts the equilibrium so that at the same extracellular concentration of flavonoid (leading to the same influx velocity), a lower intracellular one is reached; thus, under these conditions, the passive efflux velocity from the MDCK-G2 cells decreases (since it is driven by a lower concentration of flavonoid).

At equal extracellular concentrations of flavonoid, the passive influx velocities are equal in both cell lines. Because of huge difference between extracellular and intracellular volume, transport processes leading to equilibrium will not lead to a detectable change in extracellular concentration of flavonoid in a cell culture microplate well. Therefore, at equilibrium, the total efflux velocities (in MDCK-WT it is assumed to be composed only of the passive component due to the lack of expression of any known active flavonoid transporters, in MDCK-G2 it comprises both passive and ABCG2-derived active ones) are also equal:

$$V_{WTpas.eff} = V_{G2pas.eff} + V_{ABCG2}$$

Velocity of the ABCG2-mediated transport is thus equal to the difference between equilibrium velocities of passive efflux in MDCK-WT and MDCK-G2 cells. We can use the previously derived passive transport constant to express the passive efflux velocities as functions of intracellular flavonoid concentration:

$$V_{ABCG2} = V_{WTpas.eff} - V_{G2.pas.eff}$$

JPET Fast Forward. Published on September 9, 2019 as DOI: 10.1124/jpet.119.261347
This article has not been copyedited and formatted. The final version may differ from this version.

$$V_{ABCG2} = k \cdot (C_{WT} - C_{G2})$$

Therefore, by measuring intracellular flavonoid concentrations in both cell lines at a series of equal extracellular concentrations, we acquire a dataset of substrate concentration (C_{G2}) and enzyme velocity (V_{ABCG2}), allowing us to plot a Michaelis-Menten curve and fit it to experimental points using the least squares method.

$$V_{ABCG2} = \frac{V_{max} \cdot C_{G2}}{K_m + C_{G2}}$$

Where: V_{ABCG2} – ABCG2 mediated efflux velocity [μM/s], V_{max} – "maximal velocity" of ABCG2 mediated efflux [μM/s], K_m – Michaelis constant [μM], C_{G2} – intracellular flavonoid concentration in MDCK-G2 cells [μM]

Calculation of K_m and V_{max} for ABCG2 from kinetic data

Kinetic (efflux) experiments were performed as described above both for MDCK-WT and MDCK-G2, measuring intracellular flavonoid concentration at specific time points after removal of extracellular flavonoid solution. A full analytical description of flavonoid efflux kinetics in MDCK-G2 cells (where transport is both passive and active) would require an inexact numerical solution of a complex differential equation (resulting in a kinetic equation). Instead, we performed statistical analysis by non-linear regression of the velocity equation (linking transport velocity to substrate concentration). The MDCK-G2 efflux kinetics is a combination of first order passive efflux and Michaelis-Menten based active efflux. Therefore, for each time point, the expected concentration can be calculated recurrently from data for the previous time point, thus simulating the entire combined curve. This curve then undergoes non-linear regression using a four parameter equation:

$$C_t = C_{t-1} - \left[V_{ABCG2} + V_{pas.eff}\right] \cdot \Delta t$$

$$C_t = C_{t-1} - \left[\left(\frac{V_{max} \cdot C_{t-1}}{K_m + C_{t-1}}\right) + k \cdot C_{t-1}\right] \cdot \Delta t$$

C_t – flavonoid intracellular concentration at current simulated time point [μM]

C_{t-1} - flavonoid intracellular concentration at previous simulated time point [μM]

V_{max} – "maximal velocity" of ABCG2 mediated efflux [μM/s]

K_m – Michaelis constant [μM]

k – passive efflux constant [1/s]

Δt – time interval of simulation [s]

C_0 – initial intracellular flavonoid concentration (first point of simulation)

This allows the approximate calculation of enzyme constants (equation parameters) without the need to solve the differential velocity equation. Since multiple-parameter regression can lead to relatively good correlation coefficients for a wide range of parameter values, we had to set knowledge-based limits in the mathematical procedure of parameter calculation. Passive efflux constant was known (calculated previously from experiments in MDCK-WT cells), so we tested five approaches to boundary conditions in calculating Km and Vmax (implemented within the least-squares regression algorithm): fixing either of the parameters to the equilibrium experiment-derived value ("fixed Km" and "fixed Vmax"), fixing both of them ("both fixed"), allowing full computational liberty for both parameters with optimization of correlation quality ("best R^2") as well as a combined model which involved minimization of differences between calculated and assumed parameter values as well as highest possible correlation coefficient ("optimal fit").

Confocal imaging

MDCK-WT cells were seeded at a density of 25000 cells per well on thin bottom 96-well plate (SCREENSTAR, Greiner Bio-One) and incubated for 24 h. Next, cell cultures were incubated at 37°C with 20 μM quercetin solution in HBSS/BSA for 40 min. Subsequently, cells were washed briefly with cold PBS and treated with 250 μg/ml APB and 5 μM Hoechst 33342 (nuclear stain) in HBSS for 30 min in 37°C. Following one wash with HBSS, cell plasma membranes were stained for 5 min with 500 nM mCLING-ATTO 647 dye (Synaptic Systems). Images were obtained using LSM 780 confocal microscope (Zeiss) with Plan-Apochromat 63x/1.4 Oil DIC M27 objective. Nuclear fluorescence was imaged with 405 nm excitation and 415-500 nm emission range, quercetin-APB conjugate fluorescence was imaged with 490 nm excitation and 516-597 nm emission range, plasma membrane fluorescence was imaged with 645 nm excitation and 650-775 nm emission range.

Statistical analysis and curve fitting

For multiple comparisons, ANOVA was used with $p<0.05$ as the significance limit. Linear regression was performed by the standard least squares method. Non-linear regression (for exponential and hyperbolic curves) was performed iteratively using the least squares method and Microsoft Excel Solver plugin, with appropriate confidence limit (for $p<0.05$) calculations (Brown, 2001).

Results

Fluorescence calibration curves

For our experiments, three flavonoids with identical backbone and different hydroxyl group arrangement were selected (Fig. 1a) – they were all able to form fluorescent adducts with APB. Calibration curves for these fluorescent products were strongly linear across a wide range of concentrations (Fig. 1b), allowing us to calculate the fluorescence intensity coefficient (regression slope) for each flavonoid and use these values subsequently to calculate flavonoid concentration in experimental samples.

Quercetin undergoes chemical transformation in DMEM medium

Solutions of quercetin at 5 μM concentration in DMEM, HBSS or distilled water (with or without addition of 2.2 mg/ml BSA) were incubated at 37°C for different time periods, diluted 10-fold with LB and fluorescence of the APB adduct was measured (Fig. 1c). Fluorescence values (reflecting the concentration of quercetin available for conjugation with APB) remained stable in all solutions except for those in DMEM, where a steady decrease of fluorescence in time was seen (indicating a chemical transformation into a form which cannot react with APB). Presence of BSA did not affect the stability of quercetin. When an analogous experiment was performed for luteolin, fluorescence values were stable in all solutions, indicating no chemical transformation of this flavonoid.

Lysis buffer composition affects fluorescent properties of the flavonoid-APB conjugate

In order to optimize conditions for reliable measurement of intracellular flavonoid concentration, we tested the influence of potential biochemical sources of interference on measured APB conjugate fluorescence. We designed a cell-free experiment where fluorescence was measured for samples in PBS with the same final concentration of 1 μM flavonoid and 250 μg/ml APB. These samples differed by the presence or absence of Triton X-100 (0.35% final concentration), BSA (0.22 mg/ml) and the order of addition of components. The preparation scheme is depicted in Tab. 1.

When no Triton X-100 is present (sample APB), conjugate fluorescence for all flavonoids is relatively weak and significantly increases in the presence of BSA (Fig. 2a). On the other hand, the addition of surfactant also increases fluorescence with regard to the APB sample without BSA;

however, this increase is different from the BSA-mediated increase (lower in the case of quercetin and kaempferol, higher in the case of luteolin). Significantly, the impact of Triton X-100 supersedes the impact of BSA: conjugate fluorescence in Triton-containing samples is the same regardless of the presence of BSA, therefore for luteolin, fluorescence of Triton X-100+BSA samples is actually lower than that of BSA-only samples. This effect is independent on the order of addition of APB, Triton X-100 and BSA – final fluorescence intensity in the presence of Triton (samples APB/Triton, Triton/APB and LB both with and without BSA) is always the same.

Since it is apparent from the above results that BSA and Triton X-100 affect the fluorescent properties of flavonoid-APB conjugates by different and mutually exclusive mechanisms, we performed concentration titration of Triton X-100 (Fig. 2b) and BSA (Fig. 2c) at constant flavonoid and APB concentration. There is a sigmoidal dependence between Triton concentration and fluorescence, suggesting a connection to its surfactant properties and phase transitions. Indeed, the abrupt rise in fluorescence intensity starts at concentrations close to the critical micelle concentration for Triton X-100 (Rharbi *et al.*, 1999). On the other hand, the dependence between BSA concentration and fluorescence is hyperbolic, suggesting saturational binding with apparent equilibrium at 1:2 molar ratio of BSA to flavonoid.

Generation and fate of intracellular flavonoid-APB conjugates

MDCK-WT cells were loaded with quercetin in HBSS/BSA, incubated for 30 min at 37°C in HBSS/APB, stained with Hoechst 33342 (nuclear stain) and with mCLING-ATTO 647 (plasma membrane stain); subsequently, cells were imaged in the confocal microscope. The quercetin-APB conjugate localizes predominantly to intracellular structures within the cytoplasm (Fig. 3a). To test the stability of quercetin-APB conjugate distribution, cells were also incubated with quercetin and APB as above; subsequently, HBSS/APB was removed and cells were incubated for 1 h at 37°C in HBSS, nuclei and cell membraned were stained as above and cells were imaged. No significant changes in amount and distribution of the fluorescent conjugate were seen (data not shown).

Since the above result suggests that the flavonoid-APB conjugate cannot permeate the cell membrane (in contrast to its substrates – APB and flavonoid molecules, which diffuse passively through biological membranes), we performed a kinetic experiment to test this hypothesis. MDCK-

WT cells were pre-incubated for 40 min at 37°C with 15 μM quercetin in HBSS/BSA. Subsequently, cells were washed with cold PBS and incubated with HBSS or HBSS/APB. In some cases, HBSS/APB was replaced with HBSS after 10 min. After specific time periods, supernatant was removed, cells were washed with cold PBS, lysed with LB and fluorescence was measured. Concurrently, supernatant was mixed with an equal volume of 2x concentrated LB and its fluorescence was also measured. Fig. 3b shows that intracellular concentration of quercetin decreases in cells incubated in HBSS (and extracellular concentration increases concurrently), reflecting passive efflux from the pre-loaded cells. On the other hand, when APB is present, it prevents this efflux, stabilizing intracellular quercetin concentration – attesting to the fast kinetics of APB-flavonoid reaction and membrane-impermeable character of the resulting conjugate. When APB is removed after 10 min of incubation, quercetin efflux resumes, albeit at a much reduced ratio – reflecting a reduced amount of unconjugated quercetin in the cell.

Medium composition affects equilibrium concentration of flavonoids in a cell

While we proved that the presence of albumin affects the fluorescence of flavonoid-APB conjugate, it was unclear whether its presence in a cellular transport model can also impact passive flavonoid diffusion and equilibrium distribution. Therefore, we tested the impact of extracellular medium composition on equilibrium concentration of luteolin (selected as the model flavonoid in this experiment, since the previously shown propensity of quercetin to chemical transformation in DMEM would add a confounding variable to analysis). We demonstrate that the presence of extracellular protein decreases the intracellular flavonoid concentration at equilibrium (Fig. 3c), with the effect being dependent mainly on albumin concentration and independent on the presence of non-protein components: the concentration is identical if standard (lipid-containing) or fatty acid-free BSA is used, and in the case of FBS (where BSA accounts for 60% of all protein by weight) it is only slightly increased. Surprisingly, the presence of other medium components also has a drastic impact on equilibrium flavonoid concentration – it is much higher in HBSS than in DMEM. At the same time, neither protein/BSA nor other medium components influence the rate of passive diffusion itself (Fig. 3d): when equilibrium is reached in HBSS/BSA and the medium is

subsequently exchanged, the rate of decrease of intracellular flavonoid concentration is the same. Therefore, further equilibrium experiments were performed in HBSS/BSA.

Measurement of kinetic transport parameters for flavonoids

Intracellular concentration of flavonoids in MDCK-WT cells was monitored in time during efflux from pre-loaded cells. Exponential first order decay curves were fitted to experimental points in order to calculate the passive efflux constant k (Fig. 4a). The values obtained from non-linear regression were further used in subsequent calculations of enzyme-mediated transport parameters.

Km and Vmax values of ABCG2-mediated active transport of investigated flavonoids were derived from experiments involving comparison of equilibrium intracellular flavonoid concentration in MDCK-WT and MDCK-G2 cells (Fig. 4b). Michaelis-Menten curves were fitted to experimental points (intracellular concentration in MDCK-G2 cells vs. ABCG2-mediated transport velocity) and Km and Vmax values were calculated by non-linear regression for each flavonoid (Fig. 4c).

Alternative derivation of active efflux parameters from kinetic data

Since kinetics of flavonoid efflux from ABCG2-expressing cells is dependent on ABCG2 efficiency and substrate affinity, shape of the efflux curve (intracellular substrate concentrations at various times after cell pre-loading, during subsequent efflux to substrate-free extracellular solution) can also be used to derive Km and Vmax parameters for ABCG2. However, these parameters do not have a strong impact on the overall shape of the curve and their calculation from iterative non-linear regression is inherently non-exact. These approximations are made even more difficult by the interconnected character of the relevant parameters, therefore this method is more appropriate as confirmation of applicability of otherwise known parameter values (e.g. calculated from equilibrium experiments, as in our case) to efflux conditions. We demonstrate this on experimental data for quercetin transport (efflux curves from MDCK-WT and MDCK-G2 at identical extracellular quercetin concentration during equilibrium) which are used to calculate Km and Vmax by partially restricted curve fitting. Fig. 4d shows the results (regression curve and its confidence intervals) for non-linear regression by the “optimal fit”, which are in relatively good accordance with equilibrium-derived values for this substrate. Tab. 2 and Fig. 4e show the comparison of all regression approaches, with the least-restricted approach (“best R^{2}”) the only one to yield highly divergent

values, further underlining the need for knowledge-derived mathematical boundary conditions in this method and proving the value of efflux-type experiments as confirmatory rather than exploratory.

Enzyme kinetics of ABCG2-mediated transport inhibition

In order to further validate our method of kinetic parameter derivation from equilibrium experiments for practical applications, we decided to test the influence of known ABCG2 transport inhibitors (kaempferol and 5D3 antibody) on calculated Vmax and Km values for quercetin. In these experiments, MDCK-WT and MDCK-G2 cells were pre-incubated for 15 min with different inhibitor concentrations in HBSS/BSA and subsequently incubated with quercetin at various concentrations in HBSS/BSA (in the continuing presence of inhibitors) for 40 min. Further measurements and calculations were analogous to those described above for equilibrium experiments. Fig. 5a shows the measured intracellular concentrations used to calculate the difference between intracellular quercetin concentration in both cell lines. Fig. 5b shows the derived Michaelis-Menten curves. Kaempferol is a typical competitive inhibitor – therefore, it should increase Km without changing Vmax, which is supported by the shape of the experimental curves (calculated apparent Km values for 3 µM and 10 µM kaempferol inhibition are 586 µM and 1094 µM, respectively). On the other hand, 5D3 antibody (which binds to an extracellular epitope, blocking the ABCG2 protein in one conformation in its activity cycle) is a typical non-competitive inhibitor, and again the shape of experimental curves bears out this assumption (calculated apparent Vmax values for 1 µg/ml and 5 µg/ml 5D3 inhibition are 1.07 µM/s and 0.422 µM/s, respectively).

Discussion

Flavonoids are abundant dietary components with important bioactivities in the human body. Their targets and modes of action are being extensively characterized and investigated and practical therapeutic applications (both medicinal and nutriceutical) are being developed, so the question of their pharmacokinetic characteristics is highly topical (Ahn-Jarvis *et al.*, 2019; Maher, 2019; Ye *et al.*, 2019). It is well-established that ABC transporter activity in barrier tissues plays a crucial role in bioavailability and biodistribution of flavonoids and that ABCG2 is a key player in this respect (Yang *et al.*, 2012; Gonzales *et al.*, 2015; Peña-Solórzano *et al.*, 2017). Thus, reliable and broadly available methods for characterizing the interactions between flavonoids and ABCG2 are of high scientific and practical interest.

2-Aminoethyl diphenylborinate (APB) is a reagent which has seen practical use in biomedical laboratories in two entirely divergent applications: on one hand, plant biochemists have used it for colorimetric or fluorimetric detection of flavonoids, mainly in chromatography or microscopy (Saslowsky and Winkel-Shirley, 2001; Filippi *et al.*, 2015). On the other hand, it has been serendipitously identified and used as a specific inhibitor of some mammalian calcium channels (Kovacs *et al.*, 2012). As a fluorogenic substrate, its especially valuable as it diffuses quickly through biological membranes and reacts very quickly with its target compounds. Matteini at al. characterized the probable mechanism of reaction between APB and katechol or ketoenol groups in flavonoid molecules (Matteini *et al.*, 2011). Significantly, this has led us to the observation that no major mammalian metabolites seem to possess the required hydroxyl group/aromatic ring arrangement, so the background fluorescence in mammalian cells due to conjugation of endogenous compounds with APB is negligible. Based on this, in 2014 we proposed and patented the concept of using APB to measure intracellular concentration of exogenously added flavonoid in mammalian cells and of applying this to kinetic studies of ABC transporters (Studzian and Pulaski, 2017). The present paper elaborates on this concept and presents practical results obtained using this technique. Recently, there have been other reports about application of APB for measuring

exogenous flavonoids in animal cells, e.g. flow cytometric assays in cell lines (Grootaert *et al.*, 2016) as well as in vivo assays in unicellular organisms (Ferrara and Thompson, 2019).

In order to reliably characterize transport parameters of a transporter protein in whole cells, the right cellular model is crucial. Therefore, for our study we selected Madin-Darby Canine Kidney II, a polarized epithelial cell line, widely used as a model for transporter research (Mukkavilli *et al.*, 2017; Szilagyi *et al.*, 2019). While sublines of these cell overexpressing human ABCG2 were available for some time, we took advantage of the recent commercial availability of a unique variant (hu-MDCKII™) in which the endogenous canine multidrug transporters (cfABCB1 and cfABCG2) were knocked out by genetic engineering, thus removing an important confounding factor in quantitative analysis. This model retains the mammalian cellular environment (which has been demonstrated to be important for multidrug transporter activity (Telbisz *et al.*, 2007; Neumann *et al.*, 2017)) preferable to heterologous expression in lower eukaryotes (where the unpredictable background from endogenous transporters also precludes quantitative studies on non-standard substrates).

The goal of our study was the derivation of kinetic parameter values for ABCG2-mediated flavonoid transport, so a large part of our work was devoted to controls, validations and verifications of the experimental setup. APB is unique in that it passes membranes easily, but the conjugate with a flavonoid molecule is charged and does not (Matteini *et al.*, 2011). We demonstrate here that this conjugate is also not a substrate for any active or passive export systems, so once formed in the cell, it is well retained inside. This feature together with the relatively quick conjugation kinetics results in the ability to “freeze-frame” the intracellular concentration of a flavonoid for convenient kinetic measurements with good time resolution. Moreover, we were able to show that the conjugates are stable and have a broad linear fluorescence range, both preconditions for quantitative measurements. Since standard assay methods for polyphenol transport in mammalian systems involve their isolation and/or separation from the biological matrix (usually chromatography linked to mass spectrometric detection – (Li *et al.*, 2003; Hu *et al.*, 2012)), our technique is both much less labor- and time-intensive and less prone to technical artifacts.

Within careful validation of experimental parameters, we needed to investigate the effect of medium and lysis buffer components on flavonoid distribution as well as conjugate formation and fluorescence. Flavonoids are known to bind to certain proteins (including serum albumin (Dufour and Dangles, 2005; Yang *et al.*, 2008)). Our results showing that inclusion of BSA in extracellular medium leads to a shift in equilibrium distribution of flavonoid molecules inside and outside of cells were therefore expected. It is known that flavonoid binding changes it fluorescent properties (increases the quantum yield (Sengupta and Sengupta, 2003)) - we show that the APB-flavonoid conjugate also binds to albumin resulting in enhanced fluorescence output, allowing us to characterize the binding equilibrium. On the other hand, measurement of intracellular flavonoid concentration involves cell lysis and thus is necessarily done in the presence of detergents; we found that Triton X-100 also increases fluorescence emission of the conjugate, especially at concentrations above its critical micelle concentration. These results support the hypothesis of quantum yield increase by spatial stabilization (increased ring rigidity) and protection of the fluorophore moiety in the conjugate molecule, as it was suggested for endogenous quercetin fluorescence (Sengupta and Sengupta, 2003). This is further supported by the fact that if albumin and Triton X-100 are present concurrently, fluorescence output is determined exclusively by the detergent, attesting to its ability to extract the conjugate molecule from albumin and incorporate it into the micelle.

Interestingly, quercetin showed a marked time-dependent loss of the ability to form the fluorescent conjugate with APB when incubated in standard cell-culture medium (DMEM). It has been previously reported that sodium bicarbonate in cell culture medium negatively impacts quercetin stability (Hu *et al.*, 2012) – we show that this effect is limited to quercetin among studied flavonoids, is independent of the presence of albumin and is easily remedied for transport studies by using buffered saline for extracellular environment.

In a complex cellular system, active membrane transport kinetics is determined by many facets of substrate distribution. We show that the intracellularly formed conjugate is retained in the cytoplasm (as visualized microscopically) and can be reliably and easily used to calculate the (average) absolute intracellular concentration of the flavonoid at the time point of conjugation,

serving as a proxy for free substrate concentration in calculations of passive diffusion and transporter enzyme kinetics. As a necessary starting point, we used this approach to calculate first order passive diffusion constants by curve fitting of decreasing intracellular flavonoid concentration in pre-loaded cells (a standard biochemical approach when a reliable quantitative assay is available for intracellular substrate, e.g. (Ortega and Rodríguez-Navarro, 1985)). Interestingly, luteolin had the lowest passive diffusion rate of the studied molecules, despite theoretically not being the most hydrophilic molecule. In vectorial transport assay through a CaCo-2 monolayer, luteolin has previously been shown to have higher passive permeability than quercetin or keampferol (Fang *et al.*, 2017), undescoring the differences inherent to in vivo assays in various cellular models.

The main advantage of the method presented in this paper is the combination of easy and reliable determination of intracellular substrate concentrations with mathematical calculation of enzyme constants based on an additive transport model (concurrent passive and active efflux). Thus, using the equilibrium approach we were able to derive absolute values of both apparent Km (in units of average intracellular substrate concentration) and apparent Vmax (in units of reaction velocity per whole cell, independent of total protein concentration). These values are useful both for comparisons of affinity and transport efficiency between various flavonoids as well as for phenomenological flux calculations for an individual cell (e.g. in pharmacokinetic modeling of barriers composed of cell monolayers). Due to difficulties in finding a correct cellular model and technical problems with assays, there is a very limited body of literature on directly derived kinetic constants of ABCG2-mediated flavonoid transport. An et al. performed vectorial transport experiments through MDCKII monolayers (with heterologous overexpression of murine Abcg2) and concluded that kaempferol is a high-affinity, low-capacity transport substrate (An *et al.*, 2011). This agrees with our results, even though the apparent Km value calculated in the present study (ca. 36 μM) is more than an order of magnitude higher than that calculated by An et al. (ca. 1.3 μM) – this may be due both to differences in experimental design and species difference between mouse and human transporters. We also confirm the designation of luteolin as a relatively low-affinity, high-capacity ABCG2 substrate (Sadowska-Bartosz *et al.*, 2016).

The capacity of the APB method to precisely assay intracellular flavonoid concentration at defined time points (thanks to the near-instantaneous reaction kinetics) allowed us to test an alternative practical approach to derivation of kinetic constants – instead of measuring equilibrium concentrations and describing them in a zero-net-flux model, we can also perform a direct kinetic assay of substrate export to extracellular space where its concentration is negligible (due to the high dilution coefficient). Of course direct measurements at precise time points are cumbersome practically (because transport is relatively fast, short time periods after initiation are required) and require a complex mathematical approach due to the need to concurrently model two fluxes in the same direction (active and passive), but on the other hand direct detection of substrate concentration changes is a reliable, artifact-proof approach to transport kinetics. By a restricted regression method (optimal fit), we were able to obtain similar values of kinetic parameters as by the equilibrium approach, lending credence to this procedure. This method is conceptually analogous to the standard inside-out vesicle assay which depends on monitoring and mathematically fitting the changes of substrate concentration inside the vesicle (analog of extracellular space) during unidirectional transport. Thus, we are using similar mathematical flux modeling tools to derive enzyme kinetic constants as those that have been used in all major descriptions of ABCG2 activity, e.g. to derive the Km and Vmax values for its major endogenous substrate urate (Nakayama *et al.*, 2011). However, the advantage of our model is the physiological cellular setting (intact whole cell, no need to account for leak from unsealed vesicles).

We were able to validate another application of our method which provides a significant advantage to current state-of-the-art. We tested the inhibitory potency and kinetic derivation of biochemical mechanism of inhibition for two known ABCG2 blockers: kaempferol as competitive inhibitor (An *et al.*, 2011), 5D3 antibody as non-competitive inhibitor (Telbisz *et al.*, 2012; Studzian *et al.*, 2015). Our curve-fitting procedure yielded expected results, confirming the validity of this approach for classifying inhibitors. At the same time, this method has obvious advantages for practical pharmacokinetic purposes, since inhibition parameters derived in whole cells, in the presence of all intracellular components, are going to be much more physiologically relevant for modeling drug distribution in tissues and whole organism, especially with regard to barrier tissues where ABCG2

function is crucial. Since the equilibrium assay that we describe is easily amenable to miniaturization and automation, this is also a suitable approach for inhibitor screening that yields more relevant kinetic information than just inhibitory potency at individual concentrations – an avenue of further studies that we intend to pursue.

In conclusion, we developed and validated a biochemical assay for enzyme kinetics of ABCG2-mediated transport of natural flavonoids. It is interesting both for mechanistic studies of substrate recognition by this still insufficiently understood ABC transporter and practically for studies of pharmacokinetic relationship between ABCG2 (especially in its role as barrier tissue gatekeeper) and dietary flavonoids. Polyphenol compounds are natural (plant-derived) food products that also see increasing use as nutriceuticals, recommended for a large variety of ailments and ageing-related disorders due to their antioxidant capacity. Precise knowledge on their interactions with their main active transporter provides practical indications not just about their ADME parameters, but also potential food-drug interactions and personalized applications. The easy automation of this method and its relatively low cost makes it ideal for substrate screening and structure-activity relationship studies (even QSAR since calculations result in exact kinetic parameter values), which is our current further research objective.

Acknowledgments

We wish to thank Prof. J. Dastych for access to crucial equipment. We thank Prof. G. Bartosz for valuable discussions.

Authorship Contributions

Participated in research design: Rozanski, Studzian and Pulaski.

Conducted experiments: Rozanski and Studzian.

Performed data analysis: Rozanski, Studzian and Pulaski.

Wrote or contributed to the writing of the manuscript: Rozanski, Studzian and Pulaski.

References

Ahn-Jarvis JH, Parihar A, and Doseff AI (2019) Dietary Flavonoids for Immunoregulation and Cancer: Food Design for Targeting Disease. *Antioxidants (Basel)* **8**.

An G, Gallegos J, and Morris ME (2011) The bioflavonoid kaempferol is an Abcg2 substrate and inhibits Abcg2-mediated quercetin efflux. *Drug Metab Dispos* **39**:426–432.

Brown AM (2001) A step-by-step guide to non-linear regression analysis of experimental data using a Microsoft Excel spreadsheet. *Comput Methods Programs Biomed* **65**:191–200.

Dufour C, and Dangles O (2005) Flavonoid-serum albumin complexation: determination of binding constants and binding sites by fluorescence spectroscopy. *Biochim Biophys Acta* **1721**:164–173.

Ernst O, and Zor T (2010) Linearization of the bradford protein assay. *J Vis Exp*, doi: 10.3791/1918.

Fang Y, Cao W, Xia M, Pan S, and Xu X (2017) Study of Structure and Permeability Relationship of Flavonoids in Caco-2 Cells. *Nutrients* **9**.

Ferrara BT, and Thompson EP (2019) A method for visualizing fluorescence of flavonoid therapeutics in vivo in the model eukaryote Dictyostelium discoideum. *BioTechniques* **66**:65–71.

Filippi A, Petrussa E, Peresson C, Bertolini A, Vianello A, and Braidot E (2015) In vivo assay to monitor flavonoid uptake across plant cell membranes. *FEBS Open Bio* **5**:748–752.

Ford RC, and Beis K (2019) Learning the ABCs one at a time: structure and mechanism of ABC transporters. *Biochem Soc Trans* **47**:23–36.

Fraga CG, Croft KD, Kennedy DO, and Tomás-Barberán FA (2019) The effects of polyphenols and other bioactives on human health. *Food Funct* **10**:514–528.

Gantner ME, Peroni RN, Morales JF, Villalba ML, Ruiz ME, and Talevi A (2017) Development and Validation of a Computational Model Ensemble for the Early Detection of BCRP/ABCG2 Substrates during the Drug Design Stage. *J Chem Inf Model* **57**:1868–1880.

Ge S, Yin T, Xu B, Gao S, and Hu M (2016) Curcumin Affects Phase II Disposition of Resveratrol Through Inhibiting Efflux Transporters MRP2 and BCRP. *Pharm Res* **33**:590–602.

Glavinas H, Kis E, Pál A, Kovács R, Jani M, Vági E, Molnár E, Bánsághi S, Kele Z, Janáky T, Báthori G, von Richter O, Koomen G-J, and Krajcsi P (2007) ABCG2 (breast cancer resistance protein/mitoxantrone resistance-associated protein) ATPase assay: a useful tool to detect drug-transporter interactions. *Drug Metab Dispos* **35**:1533–1542.

Gonzales GB, Smagghe G, Grootaert C, Zotti M, Raes K, and Van Camp J (2015) Flavonoid interactions during digestion, absorption, distribution and metabolism: a sequential structure-activity/property relationship-based approach in the study of bioavailability and bioactivity. *Drug Metab Rev* **47**:175–190.

Grootaert C, Gonzales GB, Vissenaekens H, Van de Wiele T, Raes K, Smagghe G, and Van Camp J (2016) Flow Cytometric Method for the Detection of Flavonoids in Cell Lines. *J Biomol Screen* **21**:858–865.

Hu J, Xu T, and Cheng Y (2012) NMR Insights into Dendrimer-Based Host–Guest Systems. *Chem Rev* **112**:3856–3891.

International Transporter Consortium, Giacomini KM, Huang S-M, Tweedie DJ, Benet LZ, Brouwer KLR, Chu X, Dahlin A, Evers R, Fischer V, Hillgren KM, Hoffmaster KA, Ishikawa T, Keppler D, Kim RB, Lee CA, Niemi M, Polli JW, Sugiyama Y, Swaan PW, Ware JA, Wright SH, Yee SW, Zamek-Gliszczynski MJ, and Zhang L (2010) Membrane transporters in drug development. *Nat Rev Drug Discov* **9**:215–236.

Iorio AL, Ros M da, Fantappiè O, Lucchesi M, Facchini L, Stival A, Becciani S, Guidi M, Favre C, Martino M de, Genitori L, and Sardi I (2016) Blood-Brain Barrier and Breast Cancer

Resistance Protein: A Limit to the Therapy of CNS Tumors and Neurodegenerative Diseases. *Anticancer Agents Med Chem* **16**:810–815.

Iriti M, Kubina R, Cochis A, Sorrentino R, Varoni EM, Kabała-Dzik A, Azzimonti B, Dziedzic A, Rimondini L, and Wojtyczka RD (2017) Rutin, a Quercetin Glycoside, Restores Chemosensitivity in Human Breast Cancer Cells. *Phytother Res* **31**:1529–1538.

Kovacs G, Montalbetti N, Simonin A, Danko T, Balazs B, Zsembery A, and Hediger MA (2012) Inhibition of the human epithelial calcium channel TRPV6 by 2-aminoethoxydiphenyl borate (2-APB). *Cell Calcium* **52**:468–480.

Li F, Howard KD, and Myers MJ (2017) Influence of P-glycoprotein on the disposition of fexofenadine and its enantiomers. *J Pharm Pharmacol* **69**:274–284.

Li Y, Shin YG, Yu C, Kosmeder JW, Hirschelman WH, Pezzuto JM, and van Breemen RB (2003) Increasing the throughput and productivity of Caco-2 cell permeability assays using liquid chromatography-mass spectrometry: application to resveratrol absorption and metabolism. *Comb Chem High Throughput Screen* **6**:757–767.

Maher P (2019) The Potential of Flavonoids for the Treatment of Neurodegenerative Diseases. *Int J Mol Sci* **20**.

Mao Q (2008) BCRP/ABCG2 in the placenta: expression, function and regulation. *Pharm Res* **25**:1244–1255.

Matteini P, Agati G, Pinelli P, and Goti A (2011) Modes of complexation of rutin with the flavonoid reagent diphenylborinic acid 2-aminoethyl ester. *Monatsh Chem* **142**:885.

Mukkavilli R, Jadhav G, and Vangala S (2017) Evaluation of Drug Transport in MDCKII-Wild Type, MDCKII-MDR1, MDCKII-BCRP and Caco-2 Cell Lines. *Curr Pharm Biotechnol* **18**:1151–1158.

Nakayama A, Matsuo H, Takada T, Ichida K, Nakamura T, Ikebuchi Y, Ito K, Hosoya T, Kanai Y, Suzuki H, and Shinomiya N (2011) ABCG2 is a high-capacity urate transporter and its genetic impairment increases serum uric acid levels in humans. *Nucleosides Nucleotides Nucleic Acids* **30**:1091–1097.

Neumann J, Rose-Sperling D, and Hellmich UA (2017) Diverse relations between ABC transporters and lipids: An overview. *Biochim Biophys Acta Biomembr* **1859**:605–618.

Ortega MD., and Rodríguez-Navarro A (1985) Potassium and Rubidium Effluxes in Saccharomyces cerevisiae. *Zeitschrift für Naturforschung C* **40**:721–725.

Passamonti S, Terdoslavich M, Franca R, Vanzo A, Tramer F, Braidot E, Petrussa E, and Vianello A (2009) Bioavailability of flavonoids: a review of their membrane transport and the function of bilitranslocase in animal and plant organisms. *Curr Drug Metab* **10**:369–394.

Pedersen JM, Khan EK, Bergström CAS, Palm J, Hoogstraate J, and Artursson P (2017) Substrate and method dependent inhibition of three ABC-transporters (MDR1, BCRP, and MRP2). *Eur J Pharm Sci* **103**:70–76.

Peña-Solórzano D, Stark SA, König B, Sierra CA, and Ochoa-Puentes C (2017) ABCG2/BCRP: Specific and Nonspecific Modulators. *Med Res Rev* **37**:987–1050.

Rharbi Y, Kitaev V, Winnik MA, and Hahn KG (1999) Characterizing Aqueous Micellar Triton X-100 Solutions of a Fluorescent Model Triglyceride. *Langmuir* **15**:2259–2266.

Robey RW, Ierano C, Zhan Z, and Bates SE (2011) The challenge of exploiting ABCG2 in the clinic. *Curr Pharm Biotechnol* **12**:595–608.

Sadowska-Bartosz I, Grębowski J, Kępka E, Studzian M, Bartosz G, and Pułaski Ł (2016) ABCB1-overexpressing MDCK-II cells are hypersensitive to 3-bromopyruvic acid. *Life Sci* **162**:138–144.

Saslowsky D, and Winkel-Shirley B (2001) Localization of flavonoid enzymes in Arabidopsis roots. *Plant J* **27**:37–48.

Sawangrat K, Yamashita S, Tanaka A, Morishita M, Kusamori K, Katsumi H, Sakane T, and Yamamoto A (2019) Modulation of Intestinal Transport and Absorption of Topotecan, a BCRP Substrate, by Various Pharmaceutical Excipients and Their Inhibitory Mechanisms of BCRP Transporter. *J Pharm Sci* **108**:1315–1325.

Schutte ME, Freidig AP, van de Sandt JJM, Alink GM, Rietjens IMCM, and Groten JP (2006) An in vitro and in silico study on the flavonoid-mediated modulation of the transport of 2-amino-1-methyl-6-phenylimidazo[4,5-b]pyridine (PhIP) through Caco-2 monolayers. *Toxicol Appl Pharmacol* **217**:204–215.

Sengupta B, and Sengupta PK (2003) Binding of quercetin with human serum albumin: a critical spectroscopic study. *Biopolymers* **72**:427–434.

Shugarts S, and Benet LZ (2009) The Role of Transporters in the Pharmacokinetics of Orally Administered Drugs. *Pharm Res* **26**:2039–2054.

Sjöstedt N, Holvikari K, Tammela P, and Kidron H (2017) Inhibition of Breast Cancer Resistance Protein and Multidrug Resistance Associated Protein 2 by Natural Compounds and Their Derivatives. *Mol Pharm* **14**:135–146.

Studzian M, Bartosz G, and Pulaski L (2015) Endocytosis of ABCG2 drug transporter caused by binding of 5D3 antibody: trafficking mechanisms and intracellular fate. *Biochim Biophys Acta* **1853**:1759–1771.

Studzian M, and Pulaski L (2017) Method of Studying Abcg2 Protein Activity and Use of 2-Aminoethyl Diphenylborinate. European patent: EP3117212.

Szilagyi JT, Gorczyca L, Brinker A, Buckley B, Laskin JD, and Aleksunes LM (2019) Placental BCRP/ABCG2 Transporter Prevents Fetal Exposure to the Estrogenic Mycotoxin Zearalenone. *Toxicol Sci* **168**:394–404.

Taylor NMI, Manolaridis I, Jackson SM, Kowal J, Stahlberg H, and Locher KP (2017) Structure of the human multidrug transporter ABCG2. *Nature* **546**:504–509.

Telbisz Á, Hegedüs C, Özvegy-Laczka C, Goda K, Várady G, Takáts Z, Szabó E, Sorrentino BP, Váradi A, and Sarkadi B (2012) Antibody binding shift assay for rapid screening of drug interactions with the human ABCG2 multidrug transporter. *Eur J Pharm Sci* **45**:101–109.

Telbisz A, Müller M, Ozvegy-Laczka C, Homolya L, Szente L, Váradi A, and Sarkadi B (2007) Membrane cholesterol selectively modulates the activity of the human ABCG2 multidrug transporter. *Biochim Biophys Acta* **1768**:2698–2713.

Williamson G, Kay CD, and Crozier A (2018) The Bioavailability, Transport, and Bioactivity of Dietary Flavonoids: A Review from a Historical Perspective. *Comprehensive Reviews in Food Science and Food Safety* **17**:1054–1112.

Xiang D, Fan L, Hou X-L, Xiong W, Shi C-Y, Wang W-Q, and Fang J-G (2018) Uptake and Transport Mechanism of Dihydromyricetin Across Human Intestinal Caco-2 Cells. *J Food Sci* **83**:1941–1947.

Xie J-D, Huang Y, Chen D-T, Pan J-H, Bi B-T, Feng K-Y, Huang W, and Zeng W-A (2015) Fentanyl Enhances Hepatotoxicity of Paclitaxel via Inhibition of CYP3A4 and ABCB1 Transport Activity in Mice. *PLoS ONE* **10**:e0143701.

Yang Y, Hu Q, Fan Y, and Shen H (2008) Study on the binding of luteolin to bovine serum albumin. *Spectrochim Acta A Mol Biomol Spectrosc* **69**:432–436.

Yang Z, Zhu W, Gao S, Yin T, Jiang W, and Hu M (2012) Breast cancer resistance protein (ABCG2) determines distribution of genistein phase II metabolites: reevaluation of the roles of ABCG2 in the disposition of genistein. *Drug Metab Dispos* **40**:1883–1893.

Ye Q, Liu K, Shen Q, Li Q, Hao J, Han F, and Jiang R-W (2019) Reversal of Multidrug Resistance in Cancer by Multi-Functional Flavonoids. *Front Oncol* **9**:487.

Footnotes

This work was supported in part by the Polish National Science Centre [project no. 2015/19/B/NZ7/03856].

Reprint requests to: Lukasz Pulaski, Institute of Medical Biology PAS, Lodowa 106, 93-232 Lodz, Poland, lpulaski@uni.lodz.pl .

Legends for Figures

Fig. 1. (a) structures of studied flavonoids, (b) fluorescence calibration curves for APB conjugates of studied flavonoids, n=3, mean+SD, (c) stability of quercetin and luteolin in various solutions, n=3, mean+SD.

Fig. 2. (a) fluorescence intensity of flavonoid-APB conjugates under different reaction conditions; n=3, mean+SD, *P < 0.05 (Dunnett post hoc test vs. LB in PBS/BSA); (b) dependence of fluorescence intensity of quercetin-APB on Triton X-100 concentration; vertical lines – range of Triton X-100 critical micelle concentration (Rharbi *et al.*, 1999); (c) dependence of fluorescence intensity of quercetin-APB on BSA concentration.

Fig. 3. (a) localization of quercetin-APB conjugate (green) in MDCK-WT cells; plasma membrane stained red (mCLING-ATTO 647); nuclei stained blue (Hoechst 33342). Scale bars: 20 μm; (b) intra-/extracellular concentration of APB-quercetin during efflux in the presence and absence of extracellular APB; n=6, mean+SD; (c) equilibrium concentration of luteolin inside MDCK-WT cells in the presence of 20 μM luteolin and other additives outside the cell; n=6, mean+SD, ns P>0.05 (Tukey post hoc test). (d) passive efflux of luteolin to different media; n=6, mean+SD.

Fig. 4. (a) passive efflux of flavonoids from MDCK-WT; n=6-11, mean+SD; dashed line – fitted first order kinetic curve, solid lines – 95% confidence intervals; (b) equilibrium intracellular concentrations of flavonoids in MDCK-WT and MDCK-G2 cells. n=16, 3, 8 respectively, mean+SD; (c) Michaelis-Menten plots for tested flavonoids; n=16, 3, 8 respectively, mean+SEM; dashed line – fitted Michaelis-Menten curve, solid lines – 95% confidence intervals, vertical dotted line – K_m; (d) efflux of quercetin from MDCK-WT and MDCK-G2 cells; n=3, mean+SD; dashed line – fitted first order kinetic curve (for WT cells) or combined model optimal fit curve (for G2 cells), solid lines – 95% confidence intervals; (e) fitted curves for different statistical models (described in “Materials and methods”).

Fig. 5. (a) equilibrium intracellular concentrations of quercetin in MDCK-WT and MDCK-G2 cells in the absence and presence of inhibitors; n=6, mean+SD; (b) Michaelis-Menten plots for quercetin transport in the presence of inhibitors. C - control; n=6, mean+SEM.

JPET Fast Forward. Published on September 9, 2019 as DOI: 10.1124/jpet.119.261347
This article has not been copyedited and formatted. The final version may differ from this version.

Tables

Table 1. Order of addition of reaction components for experiment on influence of lysis buffer composition on flavonoid-APB conjugate fluorescence.

Sample name	**solution 1**			**solution 2**	
APB	200 µl APB (500 µg/ml)	+ 10 µl 40 uM flavonoid solution (in PBS or PBS/BSA)	Mix, incubate 10 min at RT	200 µl PBS	Mix, incubate 10 min at RT
APB/Triton	200 µl APB (500 µg/ml)			200 µl Triton X-100 (0.7%)	
Triton/APB	200 µl Triton X-100 (0.7%)			200 µl APB (500 µg/ml)	
LB	200 µl APB (500 µg/ml) + 200 µl Triton X-100 (0.7%)			-	

Table 2. Kinetic parameters for ABCG2-mediated transport of quercetin calculated from direct efflux experiment using different curve fitting options.

Fitting option:	K_m [μM]	V_{max} [μM/s]	R^2
Fixed V_{max}	311	**3.33**	0.9982
Fixed K_m	**137**	1.86	0.9973
Best R^2	223417	1871	0.9987
Optimal fit	195	2.36	0.9978
Both fixed	**137**	**3.33**	0.9646

JPET Fast Forward. Published on September 9, 2019 as DOI: 10.1124/jpet.119.261347
This article has not been copyedited and formatted. The final version may differ from this version.

Figures

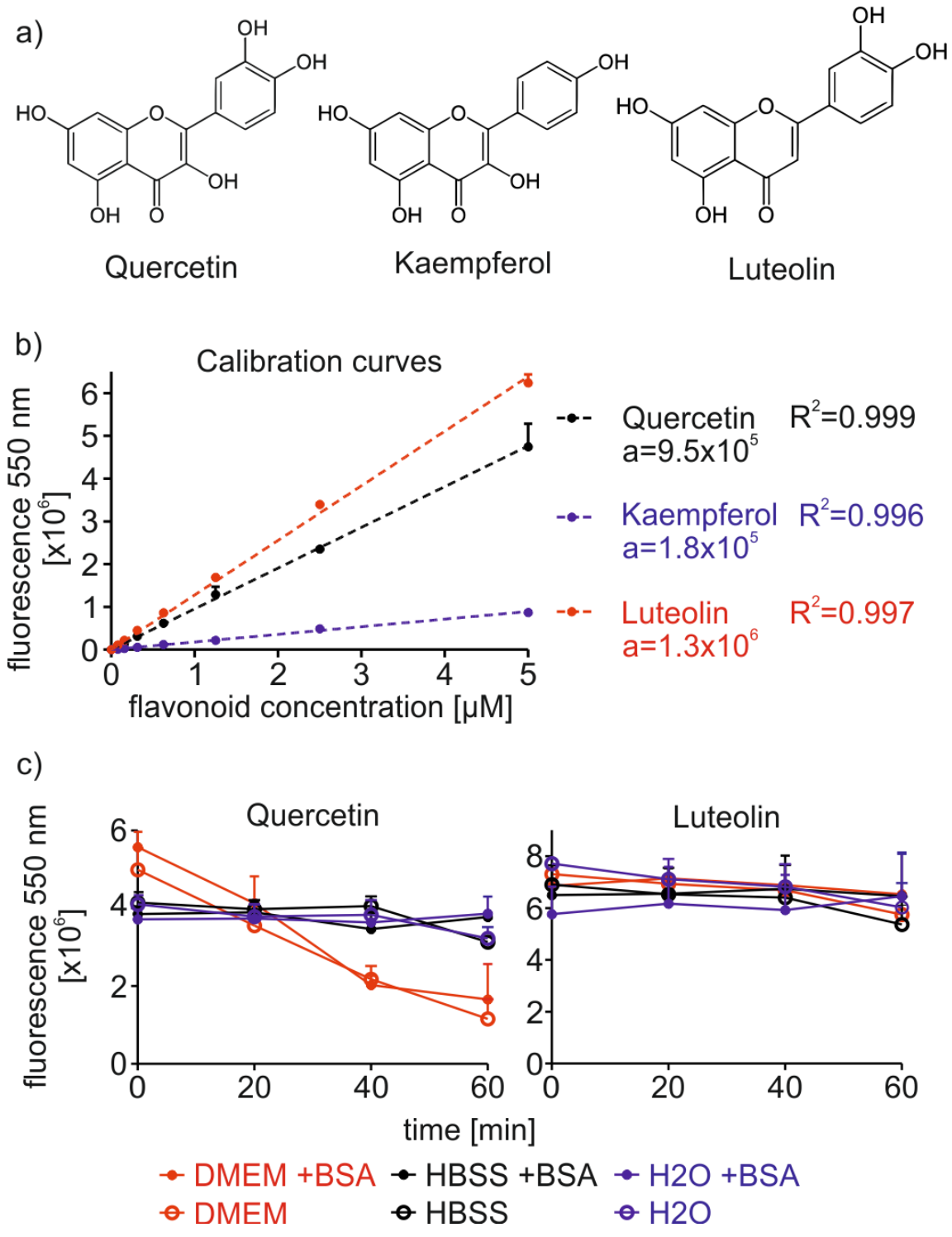

Figure 1.

JPET Fast Forward. Published on September 9, 2019 as DOI: 10.1124/jpet.119.261347
This article has not been copyedited and formatted. The final version may differ from this version.

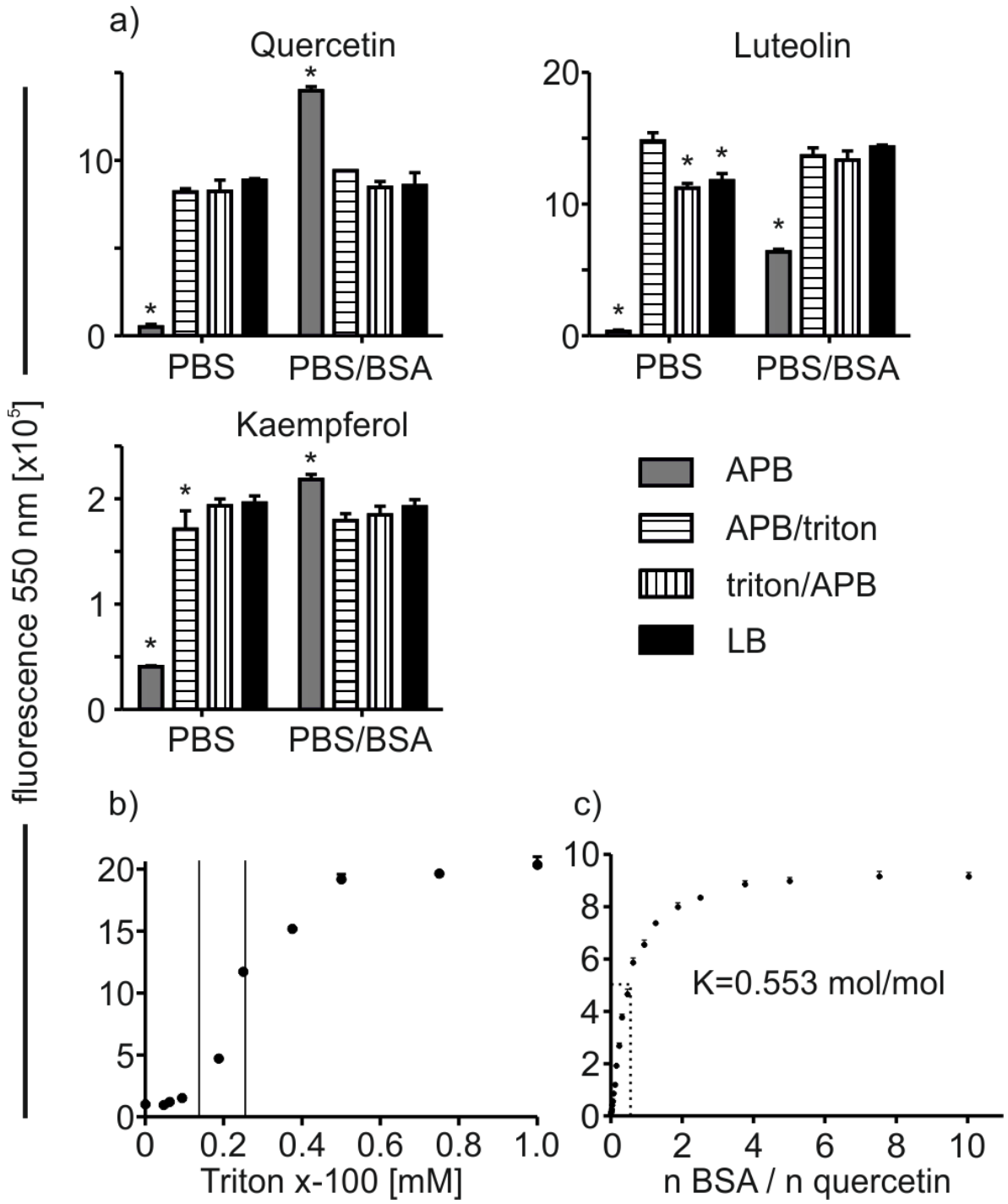

Figure 2.

JPET Fast Forward. Published on September 9, 2019 as DOI: 10.1124/jpet.119.261347
This article has not been copyedited and formatted. The final version may differ from this version.

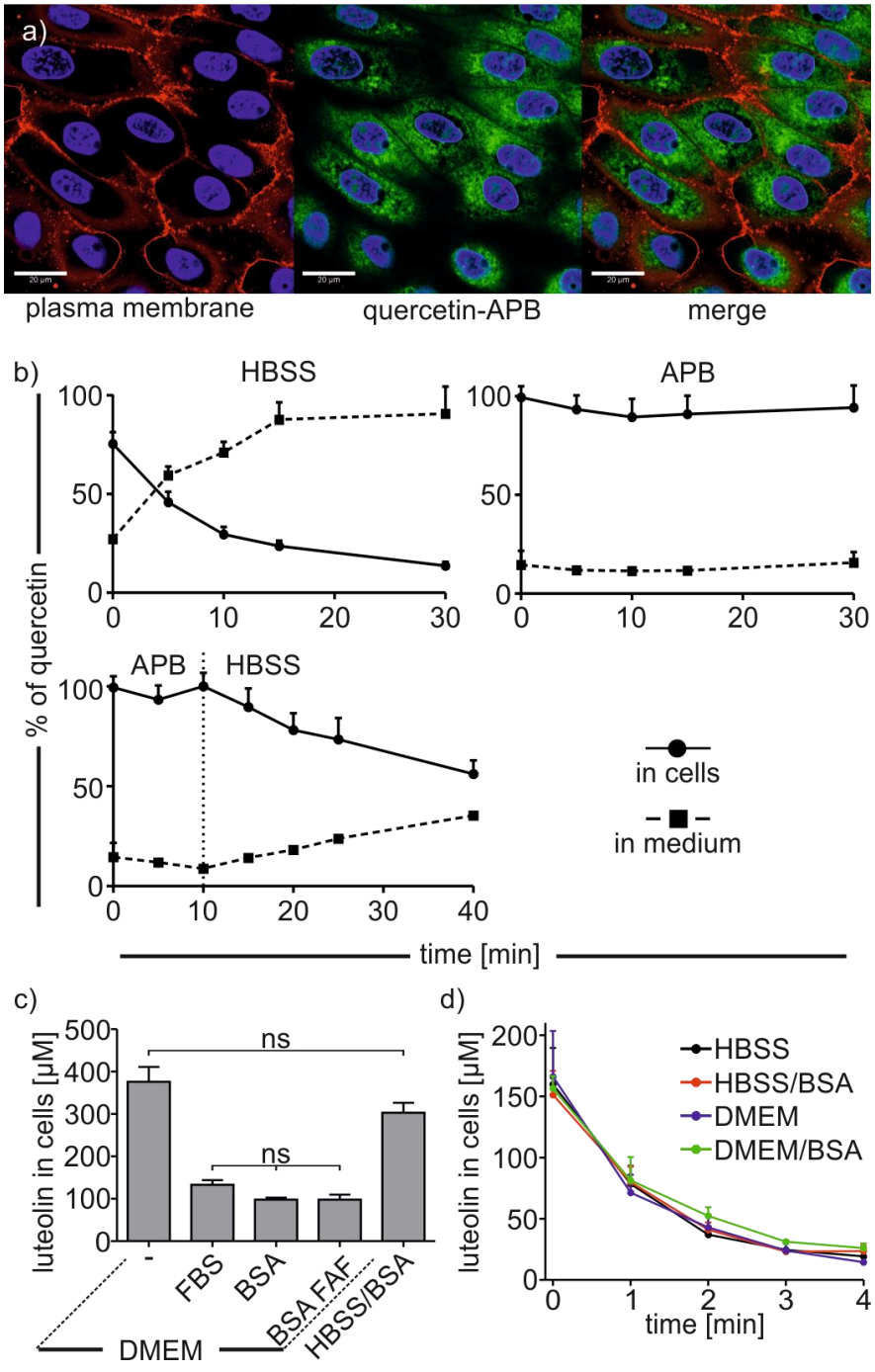

Figure 3.

JPET Fast Forward. Published on September 9, 2019 as DOI: 10.1124/jpet.119.261347
This article has not been copyedited and formatted. The final version may differ from this version.

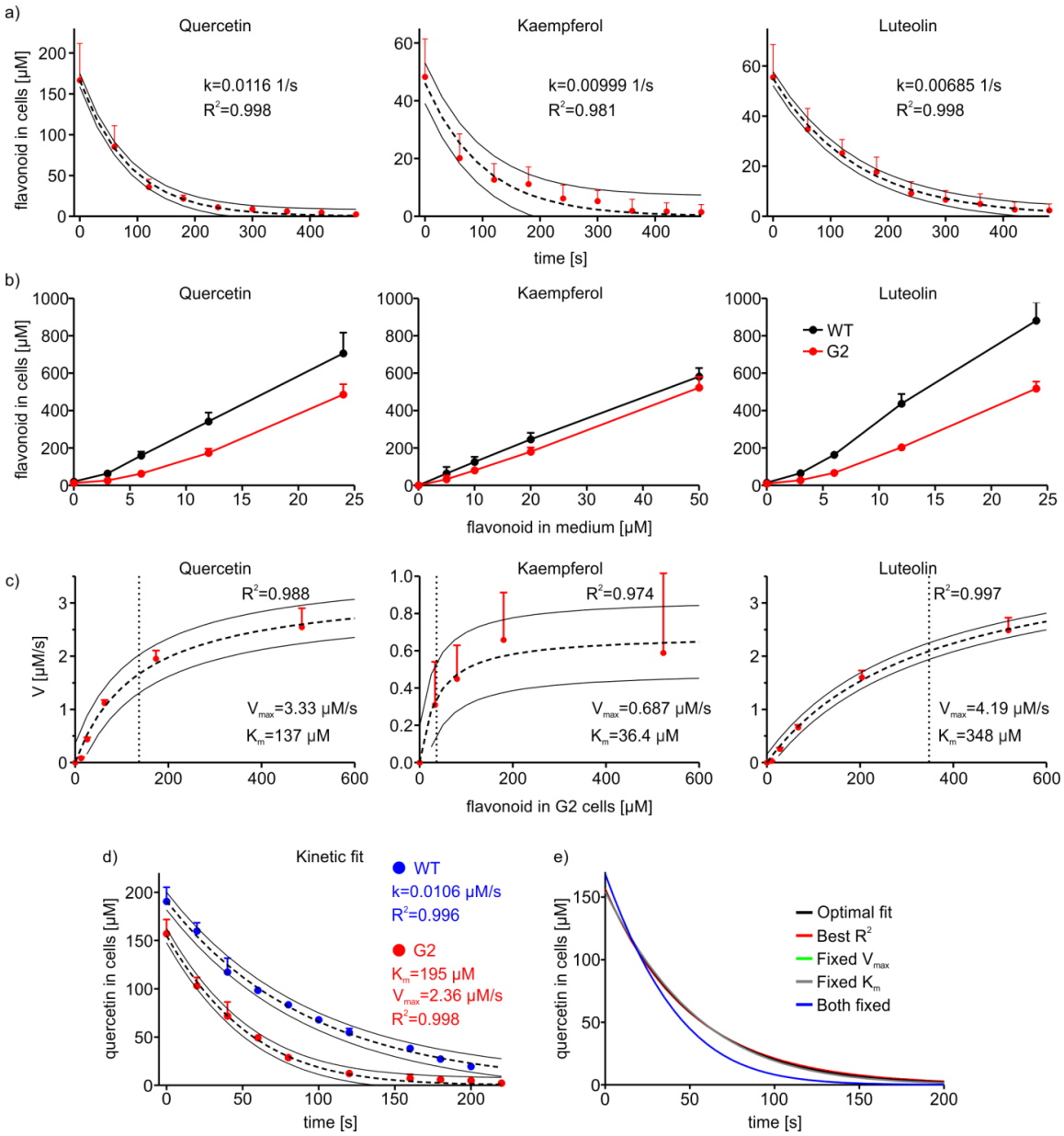

Figure 4.

JPET Fast Forward. Published on September 9, 2019 as DOI: 10.1124/jpet.119.261347
This article has not been copyedited and formatted. The final version may differ from this version.

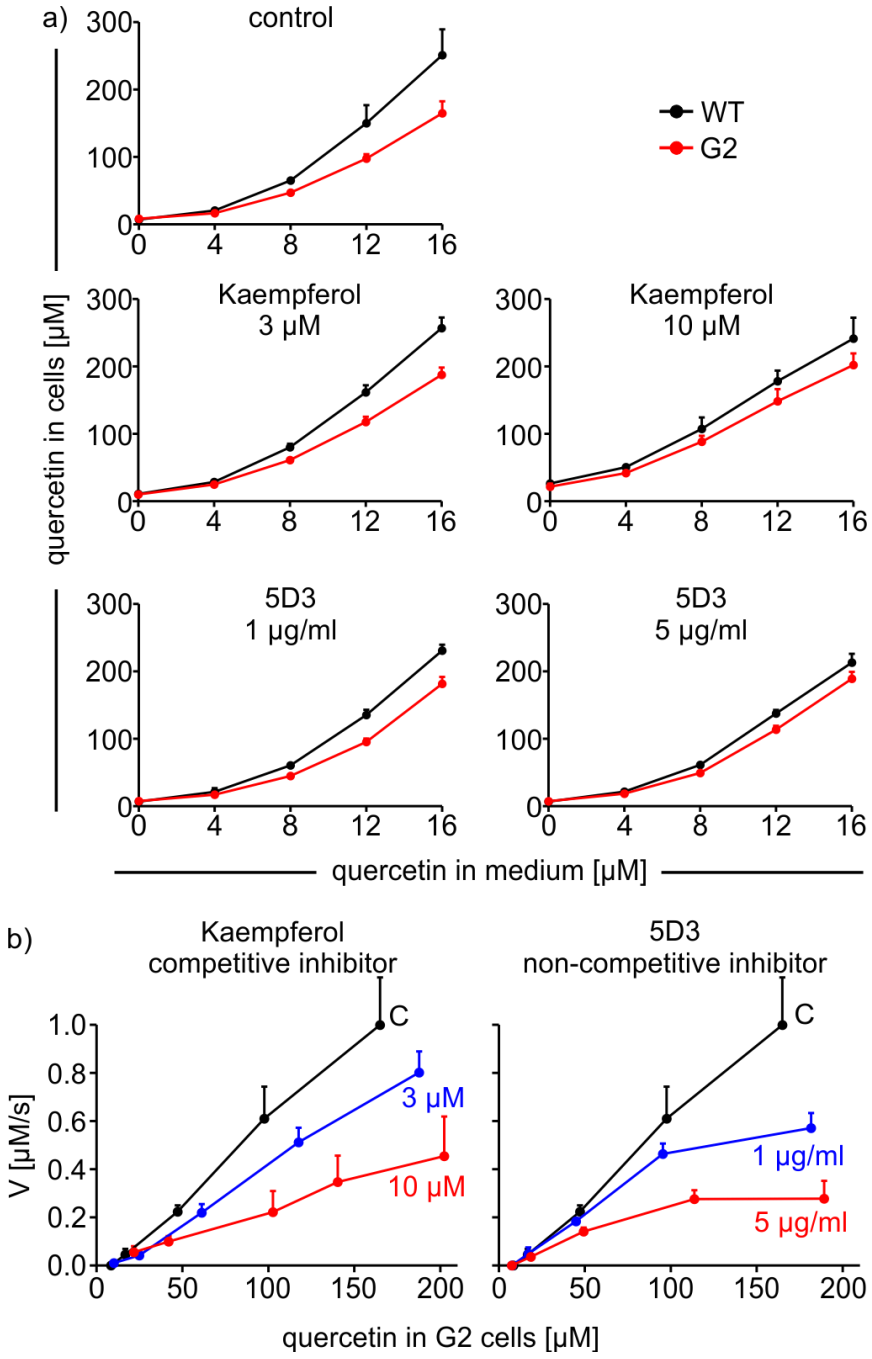

Figure 5.